Ocean Dynamics (2021) 71:237–249
https://doi.org/10.1007/s10236-020-01427-8

Seasonal variability and dynamics of coastal sea surface temperature fronts in the East China Sea

Lu Cao[1] · Rui Tang[2] · Wei Huang[2,3] · Yuntao Wang[2]

Received: 18 December 2019 / Accepted: 22 November 2020 / Published online: 7 January 2021

Abstract

Fronts in coastal oceans are important mesoscale processes that relate to regional dynamics and can impact ecosystems. The daily distribution of a sea surface temperature (SST) front is obtained in the East China Sea (ECS) using 15 years of satellite observations. High frontal activities are mainly found near the coast. The spatial and temporal variability of the monthly frontal probability is subsequently investigated using an empirical orthogonal function (EOF). Seasonal variability in frontal activities is predominant for the majority of the ECS, with the highest and lowest values occurring during winter and summer, respectively. Some major fronts have been identified, such as coastal and shelf fronts. The coastal fronts can be further divided into three separate sections: near Hangzhou Bay and along the Jiangsu and Zhejiang coasts, respectively. The shelf fronts have two sections: north and south of the Changjiang River. All fronts are characterized by a prominent seasonal cycle, though their seasonalities differ. The underlying driving forces, e.g., alongshore wind, SST, and river discharge, are further analyzed for the individual fronts. River discharge is the driving factor of fronts to the south of the Hangzhou Bay along the Zhejiang coasts while wind is the main reason for the frontogenesis near and north of Hangzhou Bay. The SST largely influences the frontal dynamics for the shelf and coastal fronts to the north. This study comprehensively describes the frontal activities in the ECS and leads to a better understanding of frontogenesis in the coastal region. It is fundamentally helpful for fisheries management and has great potential for oceanic pollution control.

Keywords Front · Sea surface temperature · Wind stress · River discharge · East China Sea · Seasonal variability

1 Introduction

Oceanic fronts are generally formed at the interface of a current system or waters with different characteristics, such as temperature, salinity, or turbidity (Belkin et al. 2009). Forcing of frontogenesis largely varies, including river discharge, tidal mixing, coastal and open ocean upwelling, and surface water convergence (Legeckis 1978). A frontal zone is generally characterized by intense dynamics, particularly for the region with prominent vertical shear in velocity that can result in large turbidity, e.g., estuaries (Waddell et al. 1979). Advection of terrigenous inorganic matter aggregates near front and elevates surrounding biogeochemical and biological processes, such as the growth of plankton (Zaneveld and Pak 1979). So, the frontal area is always associated with high primary production and fishing productivity (Smith et al. 1998; Acha et al. 2004; Woodson and Litvin 2015), attracting massive attention to investigate frontogenesis throughout the global oceans. Thus, a better description of frontal activities is fundamentally important for understanding regional dynamics and ecosystems. More recently, microplastic, as a new pollutant, is investigated intensively because it is found to distribute widely in the ocean and influence the health of aquatic organisms (Browne et al. 2007). The intense dynamics near front may bring microplastics to the surface and subsequently threat the survival of the marine species (Cao et al. 2018). Thus, the study on frontogenesis is a fundamentally important topic for both open ocean and coastal area.

Responsible Editor: Jun Wei

This article is part of the Topical Collection on the *11th International Workshop on Modeling the Ocean (IWMO), Wuxi, China, 17-20 June 2019*

✉ Yuntao Wang
yuntao.wang@sio.org.cn

[1] School of Port and Transportation Engineering, Zhejiang Ocean University, Zhoushan, China

[2] State Key Laboratory of Satellite Ocean Environment Dynamics, Second Institute of Oceanography, Ministry of Natural Resources, Hangzhou, China

[3] Key Laboratory of Marine Ecosystem and Biogeochemistry, Second Institute of Oceanography, Ministry of Natural Resources, Hangzhou, China

Generation of front is largely varying in space and time. Fronts in eastern boundary currents, e.g., the California, Canary, Humboldt, and Benguela currents, are mainly generated by wind-driven upwelling (Wang et al. 2015). Some fronts in the western boundary currents, such as the Kuroshio, Gulf Stream, and East Australia currents, form because the current carries high-temperature water to high-latitude areas where the ambient temperature is low (Belkin et al. 2009). Chen et al. (2019) studied the frontogenesis on the southeastern continental shelf of Brazil and noted that wind stress curl plays an important role in driving upwelling, which subsequently induces frontal activities. Topography is also an important factor for frontogenesis that fronts can generate around the sloping topography, e.g., bottom bump and shelf-break (Chen et al. 2003; Castelao et al. 2005).

Frontal zones are characterized by ocean-atmosphere interaction because of intensive turbulence (Yu et al. 2020). The sea surface temperature (SST) can modify the wind aloft by changing the stability of the atmospheric boundary layer (O'Neill et al. 2010). A strong (weak) wind is associated with a warm (cold) SST at the respective side of the front, and the induced wind stress curl will feedback on the SST (Wang and Castelao 2016) by reducing the SST gradient and front (Chen et al. 2019). SST is decreasing with increasing latitude because of reduced solar radiation and water mass from various origins is characterized by different SST; thus, their confluence zone can generate fronts (Shi et al. 2017).

The East China Sea (ECS) in the western North Pacific Ocean covers an area greater than 70,000 km^2. The sea is mainly locating at the continental shelf with depths less than 200 m (Fig. 1a). The outer boundary is the Okinawa Trough, whose depth exceeds 1000 m. The Changjiang River (Fig. 1b), which carries a tremendous amount of freshwater and terrestrial materials, is the major freshwater input into the ECS while the Kuroshio Current (Fig. 1a) provides heat and oceanic materials originating from the open ocean. Both coastal and offshore waters can greatly impact the ECS, and frontal activities are substantially strong. A previous study showed that the frontal zone in the ECS is a favorable spawning and nursery ground for pelagic fishes (Chen 2008; Chen et al. 2009); thus, it is necessary to study frontogenesis in this area.

The ECS is dominated by a monsoon with a northerly wind during winter and southerly wind during summer (Tseng et al. 2000). During summer, the strong monsoon drives northward flow, which transports a large amount of water vapor from south Asia northward, causing a large area of rainfall or occasionally floods, increasing river discharge to the ECS (Huang et al. 2013). The movement of surface water in the ECS is also influenced by the wind stress via driving circulation and Ekman transport (Zhu et al. 2019). The alongshore component of wind stress can drive coastal upwelling during the summer monsoon (Wang et al. 2015). An opposite phenomenon is found during the winter due to the strong northerly wind and the low river discharge (Beardsley et al. 1985).

Along the coastal area of the ECS in the south of Changjiang River, there are two major currents, i.e., the Taiwan warm current and ECS coastal current (Fig. 1b). The Taiwan warm current was first discovered during the late 1950s (Guan and Chen 1964), including the inshore branch and the offshore branch (Lian et al. 2016). The inshore branch flows northward along the coast near the 50-m isobath (Fig. 1b). The offshore branch separates from the inshore one near

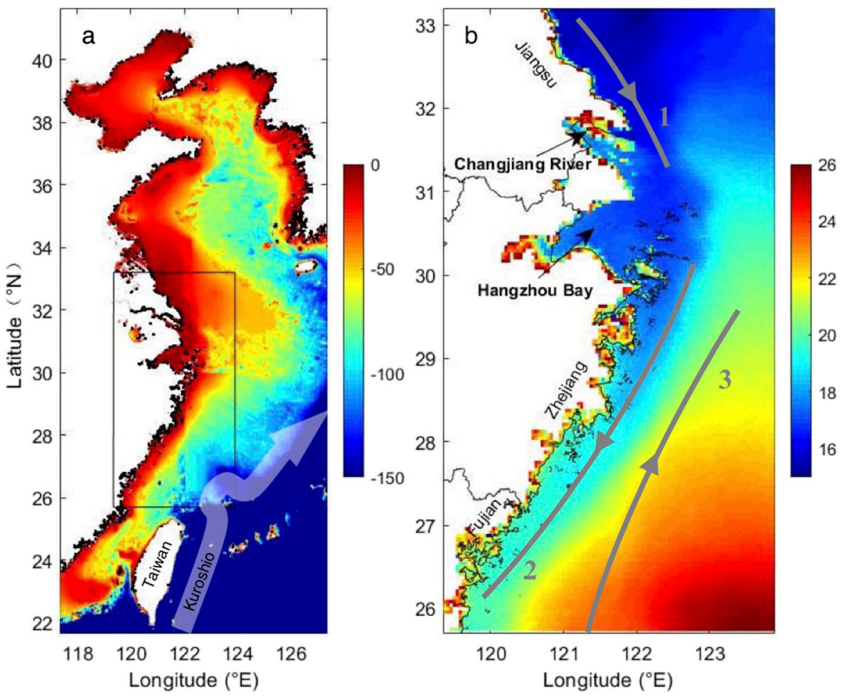

Fig. 1 **a** Topography of East China Sea (ECS) with the Kuroshio current schematically overlaid (translucent white arrow). The black box indicates the study region. **b** The climatological average of SST from 2002 to 2017 overlaid with three major currents: 1. The Yellow Sea coastal current; 2. The ECS coastal current; 3. The Taiwan warm current. The locations and rivers are labeled in panel **b**

26° N flowing along the outer boundary of the shelf, e.g., to the west of Kuroshio (Yuan et al. 1987). Its direction is stable year around, but its intensity is stronger during the summer as the current flows against northly winds during the winter (Fang et al. 1991; Zhu et al. 2004). The ECS coastal current flows persistently southward along the Zhejiang coast. In winter, the ECS coastal current, which extends southward in a narrow band along the coast, is intensified by the northern monsoon and the discharge of Changjiang River (Beardsley et al. 1985; Wu et al. 2013). While during summer, the ECS coastal current is weakened by the southern monsoon. Along the coastal area of Jiangsu to the north of Changjiang River, the Yellow Sea coastal current (Fig. 1b) is flowing southward all the year (Teague and Jacobs 2000; Hwang et al. 2014). The offshore region of ECS is mainly dominated by the Kuroshio Current, which persistently flows northeastward over the outer continental shelf towards Japan, and the subsurface water can intrude northwestward into the Zhejiang coast as far as 50-m isobath during winter (Yang et al. 2018). The complexity of the regional circulation induces a highly variable and dynamical system, including frontal activities.

Different approaches have been applied to investigate fronts, such as field observation (Briscoe et al. 1974; Marmorino et al. 1998), remotely sensed data (Cayula and Cornillon 1995), and numerical model (Marmorino et al. 1998). Su and Wang (1989) observed the plume front in the south of Changjiang River by using the observational datasets. Satellite-derived fronts in the ECS have been studied since the 1970s (Huh 1982). The spatial pattern has been greatly improved with increasing satellite resolution, such as that of the NOAA/AVHRR SST images (Hickox et al. 2000; Tseng et al. 2000; Belkin and Cornillon 2003) and Tropical Rain Measuring Mission (TRMM) microwave imager (TMI) (Huang et al. 2010). Numerical model is widely adopted to investigate the underlying dynamics of frontogenesis. For example, hydrodynamical models show that the upwelled front in the estuarine plumes is simultaneously influenced by the water flow and the wind stress (Williams et al. 2010; Rao et al. 2011).

With the development of observational approaches, the Zhejiang-Fujian coastal fronts and Jiangsu fronts were identified, and their temporal variations have been analyzed (He et al. 2016). The Zhejiang-Fujian coastal fronts are formed along the 50-m isobath, which is the boundary between the Taiwan warm current and the ECS coastal current. However, these fronts only appear during winter and disappear during summer (Zheng and Klemas 1982). He et al. (2016) noted that there are double fronts during winter off the Zhejiang-Fujian coast using satellite data and that the nearshore was generally ignored in previous studies. The Jiangsu fronts are north of the Changjiang River estuary along the coast and appear during both winter and summer (Hickox et al. 2000). However, most of the previous studies mainly describe the distribution of the fronts, and the dynamic mechanics are not fully understood. A recent study used a numerical model to simulate the coastal dynamics in the ECS and delineated the subsurface current near the bottom during winter (Yang et al. 2018). The subsurface water occasionally outcrops near the coast (Wu et al. 2017), but whether a front will be generated was not explored.

In summary, frontal activities in the ECS are fundamentally important for regional dynamics and ecosystems, but frontal variability and frontogenesis have not been well studied. Here, we comprehensively describe the variability of fronts in the ECS, including those generated along the coast and over the shelf. The underlying dynamics, e.g., wind stress, topography, and river discharge, are subsequently investigated. The remainder of this paper is organized as follows: Section 2 describes the data and method used in this study, Section 3 analyzes the results, and a comprehensive discussion is provided in Section 4.

2 Data and methods

Changjiang River discharge was obtained from the Datong station from October 2002 to September 2017. Daily observation was used with a unit of m^3/s. The SST data was obtained from the Moderate Resolution Imaging Spectroradiometer (MODIS), which had a spatial resolution of approximately 0.04° × 0.04° (Esaias et al. 1998). The wind stress was obtained using the method provided by Chelton and Freilich (2005) based on the data from the ERA-Interim reanalysis products, which were developed by the European Center for Medium-Range Weather Forecasts (ECMWF). The time span selected was from October 2002 to September 2018 for both SST and wind observations, covering 16 full years. The original spatial resolution of the wind data was approximately 0.25° × 0.25° and was interpolated to the same grid as that of the SST when comparing.

The front detection method is adopted from Castelao and Wang (2014). Briefly, the method first seeks a location with an SST gradient greater than T_1 (2.8 °C per 100 km). Then, the value of the SST gradient is assessed for the next pixel in the direction perpendicular to the SST gradient. If the gradient value is greater than T_2 (1.4 °C per 100 km), it will be marked as a frontal pixel. The procedure continues until the gradient for all the surrounding pixels is less than T_2. Then, the marked pixels are defined as a front. After obtaining the daily frontal distribution, the frontal probability (FP) is subsequently calculated for each pixel as a ratio when it is defined as a front and the time when it is cloud-free. The alongshore wind is calculated as the vector of the wind in the direction of the nearest coastline. The direction is obtained as the slope of the straight line fitting the coastline within 200 km. The local alongshore wind is the average of the wind data less than 200 km offshore (Wang et al. 2015).

In this study, the monthly intervals of the FP, wind, and river discharge are applied to identify their temporal and

spatial variability (Ullman et al. 1999) and further investigate their relationship. An empirical orthogonal function (EOF) analysis, which is widely used in atmospheric and oceanic research (Hannachi et al. 2007), is applied for describing the variability of FP. The original data are decomposed into several modes having spatial patterns and associated time series (Kaihatu et al. 1998). In this study, the first three modes of the EOF are discussed.

3 Results

3.1 Average and seasonal variability in frontal activity

The average of the FP, from October 2002 to September 2018, shows high frontal activity nearshore and decreases offshore. Several regions are characterized as high FP, particularly along the Zhejiang and Jiangsu coasts and near river mouths (Fig. 2a). Apparently, two separate fronts can be found: the coastal front immediately near the coast and the shelf front further offshore that is parallel to the coastline. The coastal fronts less than 30 km from land comprise three parts: the Jiangsu coast, Hangzhou Bay, and Zhejiang coast. The fronts near the Zhejiang coast meridionally extend from the south boundary of Zhejiang to the south of Hangzhou Bay. This frontal zone is very narrow, with a width of less than 20 km. The front in Hangzhou Bay shows a pattern from the mouth of the estuary extending to the northeast. The coastal front near Jiangsu can be found from the Changjiang River estuary expanding northwest along the Jiangsu coastline. For the shelf fronts, there is a long band distributing along the coast that can be separated into two sections by the Changjiang River estuary. Both are approximately 80 km offshore and the southern section has a higher intensity. The shelf front to the south is approximately 30 km wide. The front originates at Fujian and continuously extends along Zhejiang to the Changjiang River estuary. The north shelf front extends from the area outside of the Changjiang River estuary to the north.

The coastal fronts in the ECS show prominent seasonal variability (Fig. 3), while the corresponding variability differs for each previously mentioned frontal zone. During summer (Fig. 3d), the overall FP is at its minimum during the year. Fronts in the north, e.g., in Hangzhou Bay and near the Jiangsu coast, are reinforced. At the same time, the coastal and shelf fronts of Zhejiang are very weak or cannot be identified. Fronts start to enhance during autumn (Fig. 3a), and a distinctive frontal zone is observed along the entire shelf from Jiangsu to Fujian. The frontal activities are substantially strong in winter (Fig. 3b) when entire study region shows a prominent high value. All the fronts weaken during spring (Fig. 3c); particularly, there are nearly no frontal activities in the Hangzhou Bay. Notably, the strong frontal activities off southeast of Zhejiang are characterized by offshore migration that it initially appears as a shelf front band in autumn, enhances and widens in winter, and extends further offshore during spring.

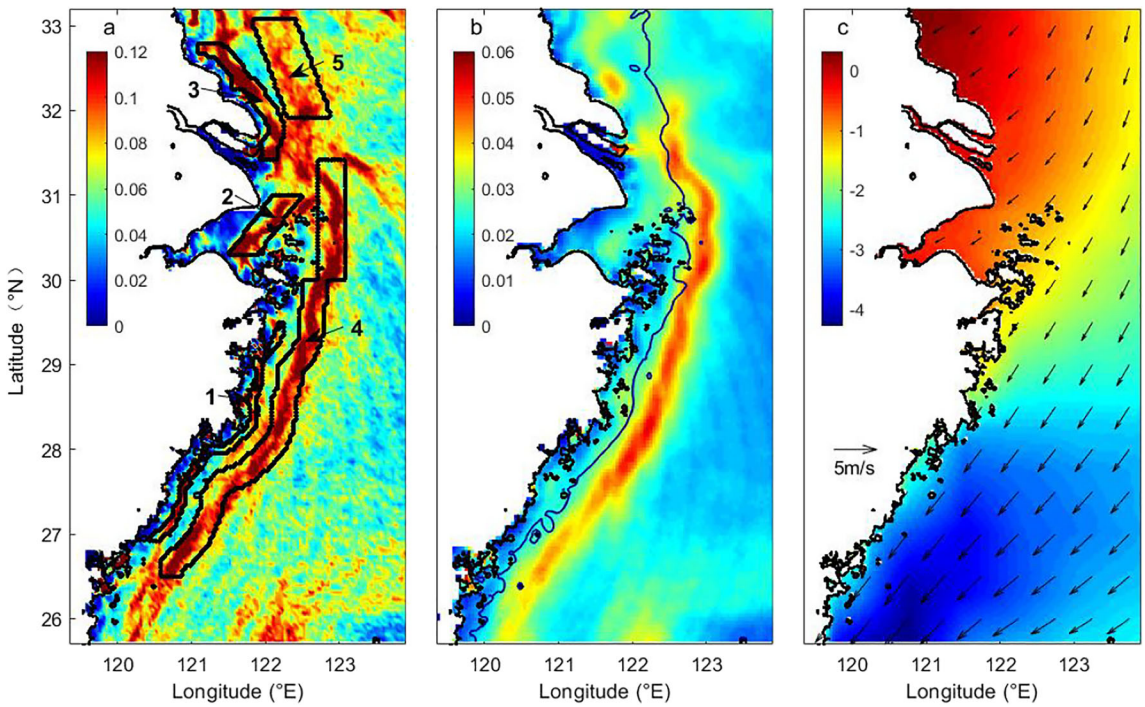

Fig. 2 Average of the (**a**) frontal probability (FP), (**b**) sea surface temperature (SST) gradient magnitude, and (**c**) alongshore wind stress with positive (negative) value indicating the wind towards north (south). The black boxes in **a** are the regions used to calculate the time series in Figs. 5, 6, 7, 8, and 9. The 20-m isobath is shown as a black contour in **b**. The unit wind vector is shown in **c**, and the unit is m/s

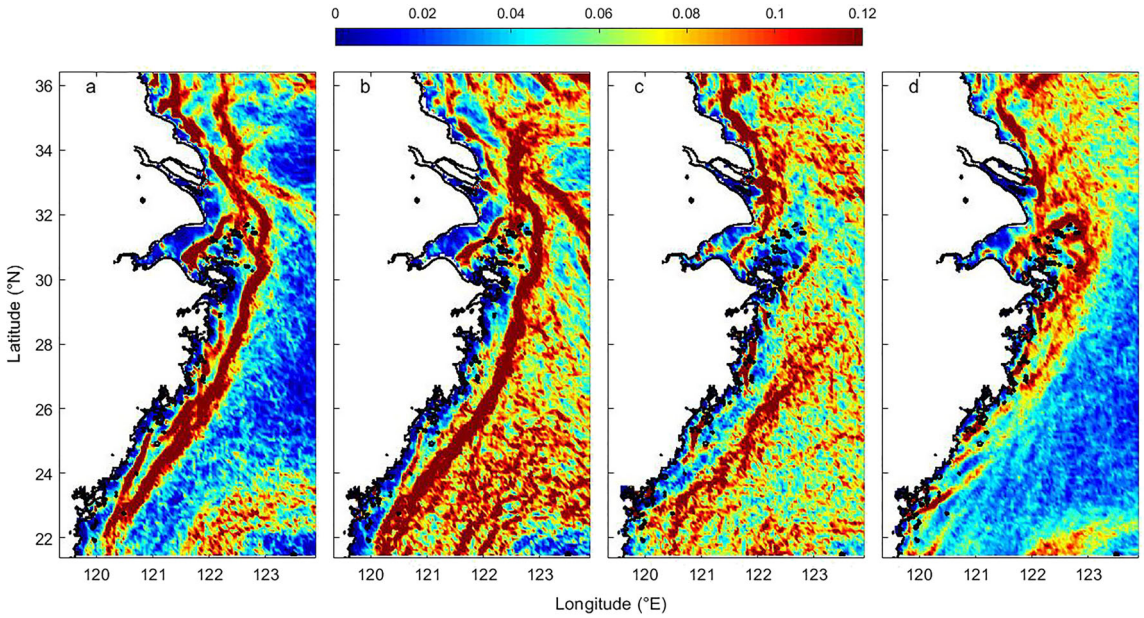

Fig. 3 Seasonal FP for (**a**) autumn (Oct.–Dec.), (**b**) winter (Jan.–Mar.), (**c**) spring (Apr.–Jun.), and (**d**) summer (Jul.–Sep.)

The dominant FP patterns are identified by EOF decompositions for the monthly time series (Fig. 4). The first three modes explain 29.1% of the total variance with each mode accounting for 14.5%, 10.3%, and 4.3%, respectively, which are comparable to previous studies (Wang et al. 2015). However, for regions with a large magnitude, the explained local variance is only about 40%, indicating that the dynamics in the study area are very complicate. EOF 1 mainly explains the variance of FP offshore of Zhejiang (Fig. 4a), which is mostly caused by the movement of Kuroshio Current and Taiwan warm current. Front activities are enhanced from February to May (Fig. 4d), which are consistent with the seasonal distribution (Fig. 3). EOF 2 captures the frontal activities near the coast and over the shelf; their corresponding magnitudes have opposite signs (Fig. 4b). Their principle components are characterized by a prominent seasonal cycle in which the shelf and coastal fronts are enhanced during autumn to winter and spring, respectively. EOF 3 mainly captures the frontal activities near the coast up to 80 km offshore with approximately the same magnitude. The time series is characterized by semiannual variability, peaking during July and December.

Combining the first three EOF, the frontal variabilities in the nearshore and offshore regions are clearly captured with different seasonality. For the nearshore region, the FP enhances during both June (EOF 2 and 3) and December (EOF 3), while the shelf front elevates during December (EOF2). In addition, the nearshore front in the area of Hangzhou Bay also shows the same seasonality as that of the shelf front. Thus, the ECS is uniquely characterized by complex dynamics and multiple mechanisms drive the frontal variability, which will be discussed in the next section.

3.2 Mean status and variability of the dynamical factors

The overall averaged alongshore wind in the study area is shown in Fig. 2c. The mean wind is characterized as northeasterly, and the alongshore wind speed is stronger south of the Changjiang River compared to that to the north. Thus, the overall wind is downwelling favorably, particularly near the Zhejiang coast. A monsoonal wind can be identified from the seasonal wind pattern (Fig. 5). Northeasterly and northerly winds dominate autumn and winter, while the wind is from the southeast during summer (Fig. 5d). The wind intensity is generally weak at high latitudes and near the coast. An air-sea interdependence can be seen in that the weak wind is associated with a low SST (Yu et al. 2020).

The average of SST is decreasing with increasing latitude (Fig. 1b), due to the solar radiation. In zonal direction, the SST is higher near the coast and further away from the coast, which may due to the cold ECS coastal current over the shelf and warm Taiwan current further offshore (Liu and Hou 2012; Wu et al. 2017). A clear seasonality can also be observed (Fig. 5). During summer, the SST in the ECS uniformly ranges between 27 and 29 °C; thus, spatial variability is not prominent. Indeed, it is difficult to find the interfaces among different SST and the weak front identified during this period (Fig. 3d). For the other seasons, SST has a greater range and the zonal SST difference is prominent, which can be captured by the SST gradient (Fig. 2b). A large gradient line along the 20-m isobath outside of the Changjiang River estuary is clearly evident (Fig. 2b).

River discharge is an important source of freshwater in the coastal area. In the ECS, the Changjiang River is the largest

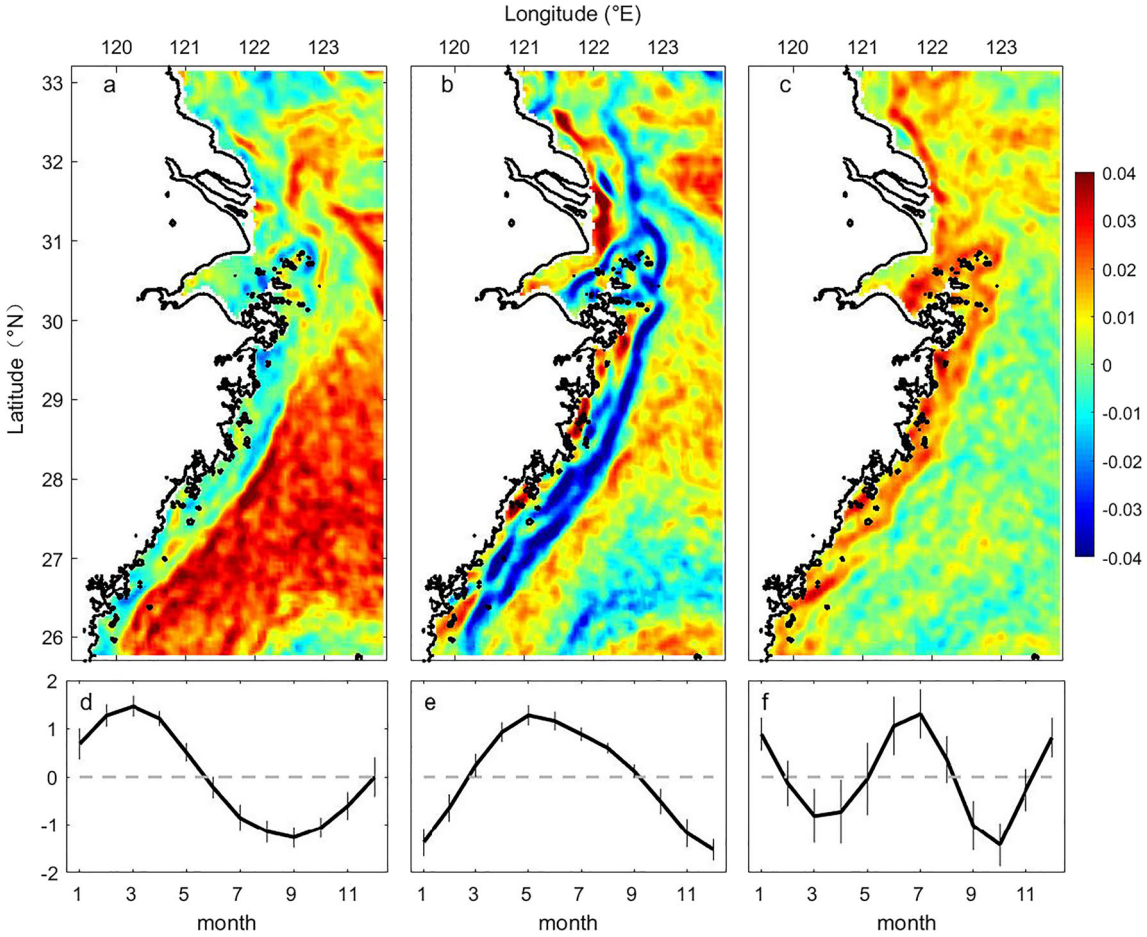

Fig. 4 Magnitude (**a**–**c**) and principal component (**d**–**f**) for the first three EOF models of frontal probability. The gray bar in **d**–**f** is the standard deviation of the principal component for each month

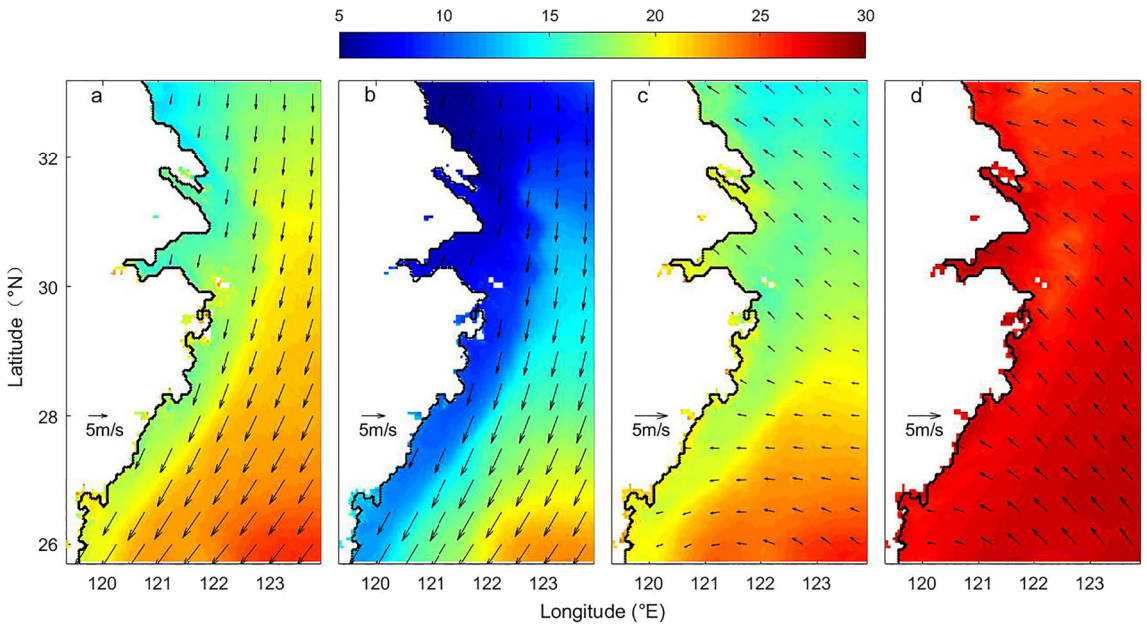

Fig. 5 Seasonal distribution of the wind (the SST is shown in color). **a** Autumn (Oct.–Dec.), **b** winter (Jan.–Mar.), **c** spring (Apr.–Jun.), and **d** summer (Jul.–Sep.)

river, contributing approximately 9×10^{11} m^3 of freshwater, accounting for 79.7% of the total freshwater input and 73.1% of the sediment input (4.8×10^{11} of 6.6×10^{11} kg) (Chen and Zhao 1985). The Changjiang River discharge shows a prominent seasonal variability, i.e., low during winter and high during summer (Fig. 6). Pan et al. (1997) noted that the Changjiang River discharge is approximately 10,000 m^3/s during winter and 50,000 m^3/s during summer. They also found that , compared to the Changjiang River, the Qiantang River only contributes 2.9% and 0.9% of the freshwater and sediment of the ECS, respectively. In this study, the coastal river discharge is represented by monthly data of Changjiang River.

3.3 Influence of the driving factor on the FP in different areas

The seasonal cycle is substantially important for understanding the variability of FP and other factors. To describe the seasonality of different factors, the data is firstly normalized by removing the overall average and divided by the corresponding standard deviation. Because the dynamic is largely varying in space, the ECS is divided into five subareas (as denoting by the black boxes in Fig. 2a) based on the EOF analysis. Areas 1 to 3 are focused on the coastal fronts, i.e., along the Zhejiang coast, Hangzhou Bay, and Jiangsu coast, respectively. Areas 4 and 5 describe the shelf fronts offshore of the Zhejiang and Jiangsu coasts, respectively. However, the prominent seasonal variability does not indicate a dynamical relationship among them; thus, a detailed analysis is conducted at an anomalous field to investigate the frontogenesis following Wang et al. (2020). The anomalous field is obtained by removing the monthly average from the time series. A linear regression method is applied for each region to quantify the relationship between the anomalous FP and other factors, such as river discharge and wind stress. Those characterized as significant correlations for each region are described as following.

For area 1, the FP time series and river discharge agree well at seasonal scale (Fig. 6a, b), and a significant linear regression (0.84) is found at their anomalous field. This result indicates the high river discharge results in a large freshwater input and the water flows southward along the coast. Because of the coastline curvature, the river discharge generally flows along the topography instead of reaching the coast (Wang et al. 2015). Thus, the cooler water can induce fronts at its boundaries near the coast and over the shelf. Apparently, inconsistencies remain between their time series. For example, another FP peak was identified during winter, but the river discharge was low. The strongest frontal activity occurs during June, while the highest river discharge occurs during July. This difference suggests that the FP in the nearshore of the Zhejiang coast not only is influenced by river discharge but also is affected by other factors. For example, the cold-water mass of the Yellow Sea coast current flows southward in winter, and it enhances the frontogenesis in area 1, though corresponding river discharge is low.

For area 2, wind is the only driving factor that has a highly significant correlation with FP (Fig. 7). The coupling coefficient for linear regression is 0.94, which is significant at a 99%

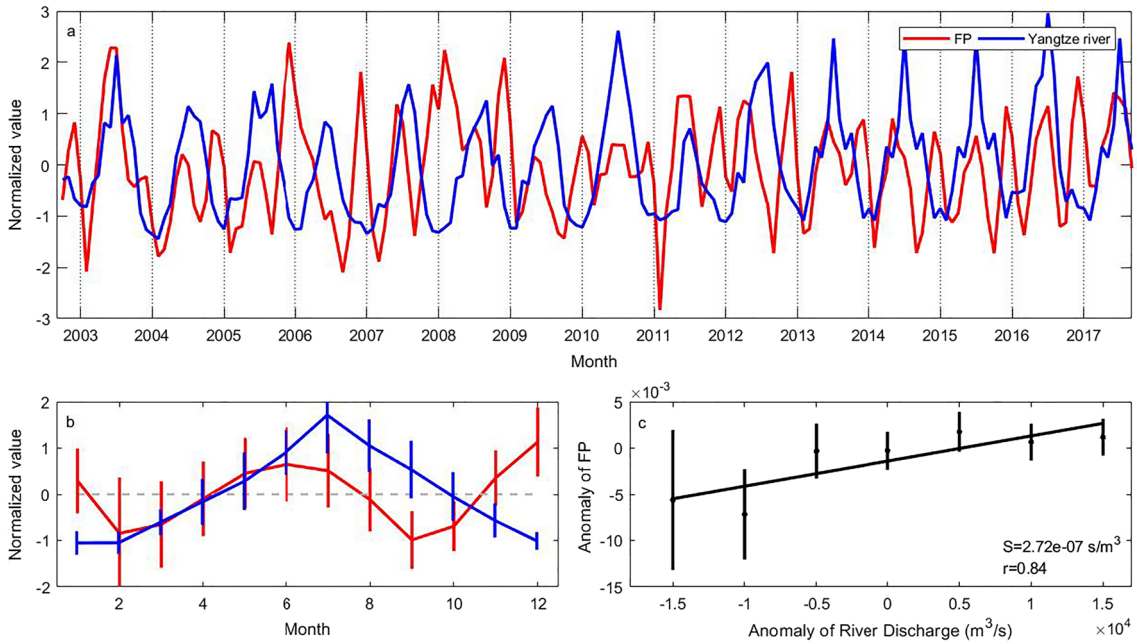

Fig. 6 For area 1, (**a**) monthly time series, (**b**) monthly average of the FP anomaly (red) and river discharge (blue), and (**c**) linear regressions between the anomalous river discharge and frontal probability. The vertical bars in **b** and **c** represent the standard deviations of the values within each bin. The coupling and correlation coefficients for the regression are labeled in **c**

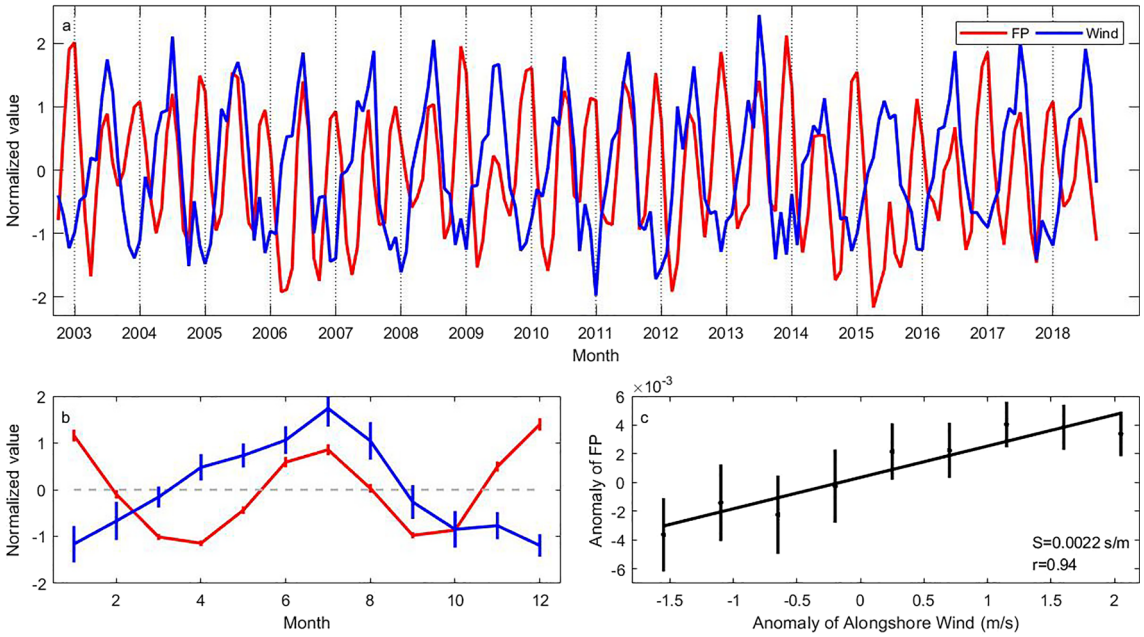

Fig. 7 Similar to Fig. 6, but for area 2. The blue lines represent the alongshore wind

confidence level. In the ECS, a northward alongshore wind can induce offshore Ekman transport, forcing the coastal subsurface water to move upward. A front is generated at the boundary between the cold upwelled water and warm offshore water. Indeed, a northward wind occurs between June and August in the ECS, when the FP is also high. During winter, there is another peak of FP being identified. It is mainly attributed to the strong southward wind that drives the cold-water mass flowing along the coast to the south, and subsequently induces frontal activities in area 2.

For areas 3 and 4, both the alongshore wind and SST show a strong correlation with the FP. For area 3, FP peaks in June and November while wind and SST peak in July and August, respectively (Fig. 8b). For area 4, the FP peaks during winter, showing an opposite seasonality to that of the wind and SST (Fig. 9b). However, a positive correlation coefficient is always found between the FP and the other factors. For example, in area 3, the correlation between the FP and wind is 0.96 ($P < 0.01$) and that between the FP and SST is 0.86 ($P < 0.01$) (Fig. 8c, d). In area 4, the correlation coefficient between the FP and wind is 0.68 ($P < 0.05$) and that between the FP and SST is 0.91 ($P < 0.01$) (Fig. 9c, d). The SST gradient in area 3 is much weaker than that of area 4 (Fig. 2b), and their locations are apart from each other. During spring and

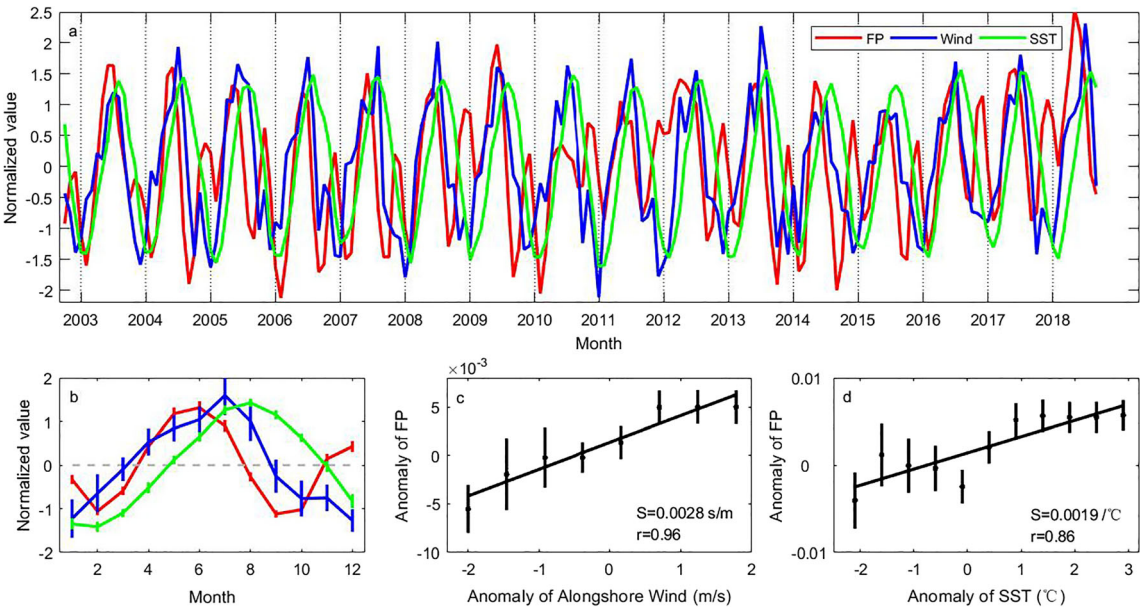

Fig. 8 Similar to Fig. 6, but for area 3. The blue lines represent the alongshore wind, and the green lines represent the SST

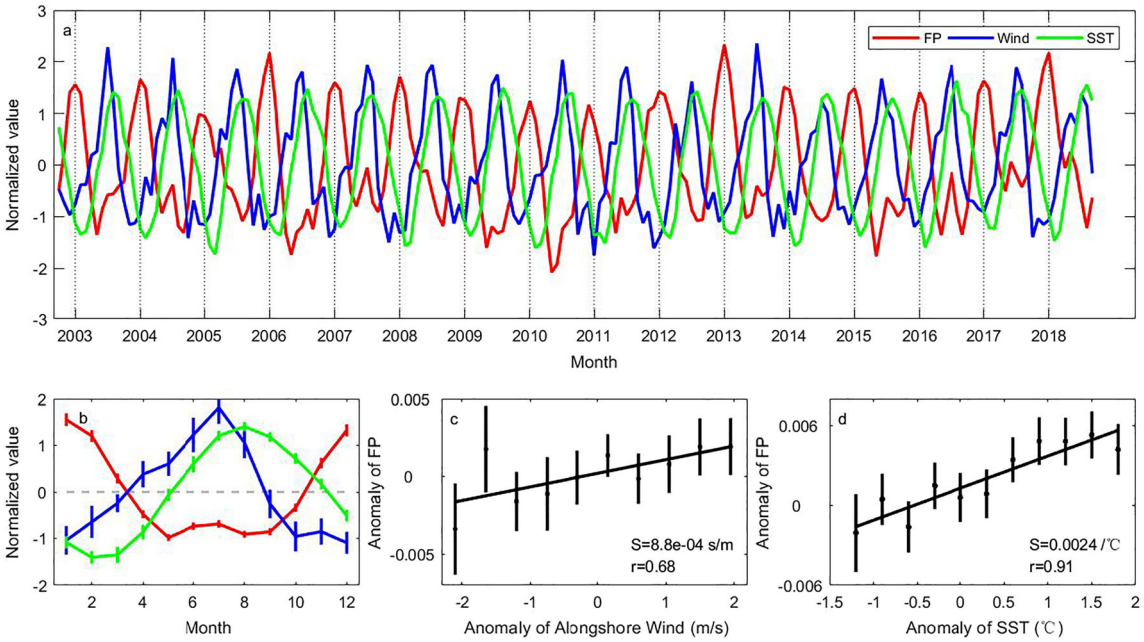

Fig. 9 Similar to Fig. 6, but for area 4. The blue lines represent the alongshore wind and the green lines represent the SST

summer, the alongshore wind in area 3 results in offshore Ekman transport and northward warm current, causing the subsurface water to outcrop and generate fronts. For area 4, the Ekman pumping induced by a spatially varied wind drives upwelling (Chen et al. 2019), which subsequently results in fronts. Regardless of area, an anomalous negative wind indicates a stronger southward wind during winter or a weaker northward wind during summer. Thus, wind-driven upwelling and Ekman pumping weaken, resulting in less frontal activity at anomalous field. While during autumn and winter, strong northly wind drives the cold water flowing southward from Yellow Sea to area 3 and 4; the lower SST induces stronger FP (Figs. 8 and 9).

Area 5 is the region over the shelf off Jiangsu where a high FP occurs around June and December at seasonal variability (Fig. 10b). A large FP in area 5 occurs during autumn and winter (Fig. 3), when the wind-driven current is flowing southward and transporting cold water along the coast (Fig. 5). Thus, the interface of the cold coastal water and warm shelf water can generate fronts (Fig. 10c). In June, the southeastly wind drives northward current, which induces warm water near the coast associating with high frontal activities in area

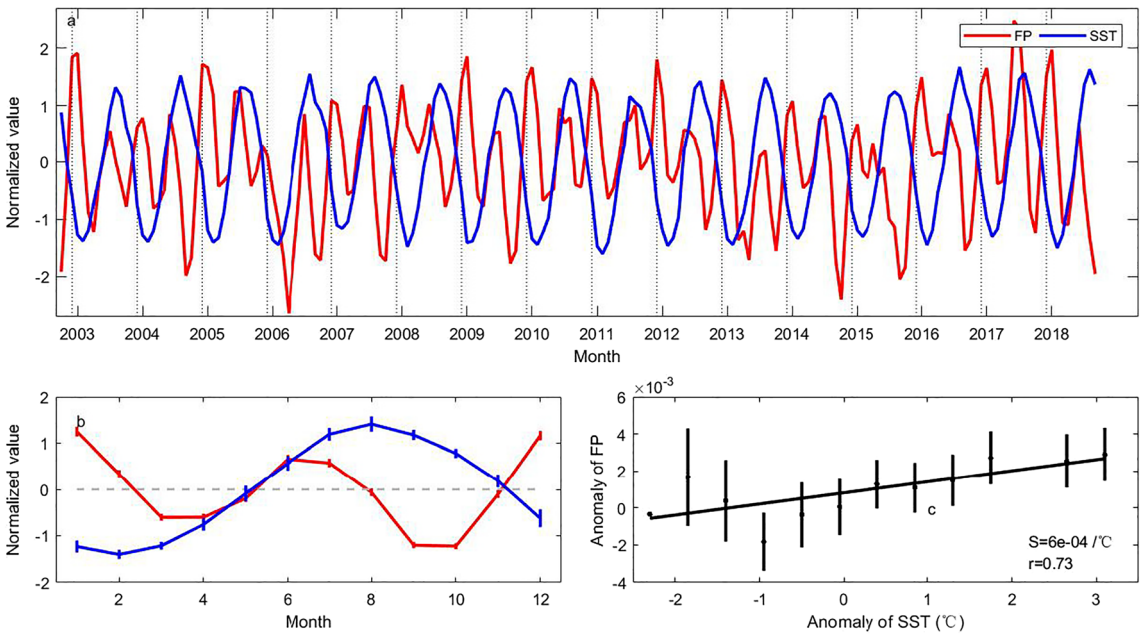

Fig. 10 Similar to Fig. 6, but for area 5. The blue lines represent the SST

5 (Fig. 5c). For both cases, there are more fronts if the SST in area 5 is warmer. Indeed, the FP is positively correlated to the SST in anomalous field with a correlation coefficient equals to 0.68, which is significant at a 95% confidence level.

4 Discussion and conclusion

Along the Zhejiang and Jiangsu coasts, two branches of fronts are observed using high-resolution satellite observations. The major frontal distribution agrees well with that of Hickox et al. (2000), and a double front feature off Zhejiang during winter is identified consistent with the recent discovery by He et al. (2016). The seasonality of the frontal activity and respective driving forces vary among regions. An EOF analysis is used to determine the major variability of the fronts, and the difference among regions can be clearly seen in Fig. 4. The ECS is further divided into five subregions (Fig. 2a), i.e., three coastal fronts and two shelf fronts, to investigate the corresponding frontogenesis. Specifically, areas 1 and 4 delineate the coastal and shelf fronts off Zhejiang, areas 3 and 5 delineate the coastal and shelf fronts off Jiangsu, and area 2 delineates the coastal front near Hangzhou Bay.

Frontogenesis is investigated by quantitatively comparing SST and wind data from October 2002 to September 2018 and river discharge data from October 2002 to September 2017. The wind pattern in the study area is dominated by a monsoonal system with a northerly wind during winter and southerly wind during summer (Tseng et al. 2000). The river discharge is predominantly determined by the Changjiang River (Pan et al. 1997). The local circulation is composed of the Taiwan warm current, the Yellow Sea coastal current, and ECS coastal water. Particularly, there is a subsurface bottom current flowing northward along the shelf during winter (Yang et al. 2018) and the Changjiang diluted water flows mainly to the northeast during summer (Beardsley et al. 1985).

The fronts generated in the estuary are highly related to the river discharge, consistent with that of the estuary of the Amazon River (Renan et al. 2009). Similarly, Castelao and Barth (2005) noted that for a front generated within 30 km from the coast in a region with simple topography, river discharge is the important dynamic factor. The freshwater discharge carries water with different salinity and temperature; thus, fronts generate as river discharge confluences with surrounding water (Table 1). Previous study pointed out that the temperature front and the salinity front are coincided well, and the SST front applied in current study can represent the frontal activities in the estuary (Kok et al. 2001). The Changjiang River is the main freshwater source for the ECS, and the ECS coastal current flows southward along the 20-m isobaths and can be enhanced by the discharge of Changjiang River. A prominent front is observed in area 1 and its activity is highly correlated with river discharge (Fig. 6), which is less dependent on surface cooling, as argued by He et al. (2016). Surprisingly, the front generated in Hangzhou Bay (area 2) is not related to the river discharge (Fig. 7). This result may be due to the regional dynamics being dominated by strong tidal and wind forces (Zhang et al. 2013).

Table 1 Correlation coefficients of each factor's anomalies to frontal probability anomalies. The correlations that are significant at 95% confidence level are indicated as italicized number

	River discharge	Wind stress	SST
Area 1	*0.84*	0.06	0.12
Area 2	0.48	*0.94*	0.41
Area 3	0.57	*0.96*	*0.86*
Area 4	0.47	*0.68*	*0.91*
Area 5	0.17	0.54	*0.68*

The front in the Hangzhou Bay (area 2) and the coastal fronts along Jiangsu (area 3) are highly correlated with the alongshore wind and impacted by the strong tidal mixing (Ma et al. 2004). During summer, due to Ekman transport, the southerly wind causes upwelling and generates fronts (Figs. 7 and 8). Similar to other upwelling systems, e.g., southeast of Brazil (Palma and Matano 2009) and the Eastern Boundary Current System (Wang et al. 2015), wind-driven upwelling is the dominant dynamic (Wang et al. 2020). Numerical simulation was applied to study the Changjiang plumes distribution and found that wind plays an important role on the movement of the river discharge via wind-induced upwelling, wind mixing, and wind-driven northward current (Xuan et al. 2012). Our result notes that the shelf front of Zhejiang (area 4) is not entirely determined by the wind pattern (Table 1). During summer, the alongshore wind can cause upwelling in this area (Wang and Wang 2007), but the SST in the ECS uniformly ranges between 27 and 29 °C (Tseng et al. 2000); this low spatial variability does not lead to front generation. Indeed, though the averaged wind is strong in summer and the FP is positively correlated to the wind in anomalous field, the overall FP is still low (Fig. 5d). On the other hand, during winter, the northerly wind can accelerate the flow of the cold ECS coastal waters, which is favorable for front generation between the ECS coast current and Taiwan warm current. Thus, there is a negative correlation between the wind and FP at a seasonal scale. However, a positive correlation still holds in the anomalous field (Figs. 7, 8, and 9). A stronger southerly wind during summer can induce more upwelling and increase front generation, while a stronger northerly wind can result in an overall cooling of the entire region and fewer fronts (Table 1).

The currents are found important for frontogenesis because the contained water character can be largely different to the surroundings. For example, there are two currents in area 4, e.g., the Taiwan warm current and the ECS coastal current.

The Taiwan warm current, which has high-temperature and salinity water, flows northeastward throughout the year, mainly between the 50- and 100-m isobaths (Su 2001). The ECS coastal current is characterized by low salinity and cold-water masses, which distributes over the region with a water depth less than 50 m. Because of the different characteristics of these currents, fronts are generated at their interfaces. During winter, cold water from the north intrudes southward into the ECS (Qiao et al. 2006) and meets the warm Taiwan current, which can enhance the fronts in area 4 (Fig. 2b, Zheng and Klemas 1982). The front in area 3 is also influenced by currents, e.g., the Yellow Sea coastal current, the cold-water flow from the north mixed with the local water, and generated front. In particular, the northerly wind enhances the cold water of the Yellow Sea current and decreases SST in winter, which induces front (Fig. 8b). Similarly, the Yellow Sea coastal current flows to the coast of ECS in autumn and winter (Fig. 5) and induces the front in area 1 and area 2.

Numerical study illustrated that a surface front is always found parallel to a coastal boundary and bottom topography (Barth 1989). In our study, area 4 is characterized as a maximum bathymetric gradient zone (MBGZ) where the topography rapidly changes (> 1 m/km). Further offshore, the water depth is greater than 50 m and slowly changes (He et al. 2016). The bump in topography can induce regional recirculation and convergence, which is favorable for generating fronts in the surrounding waters (Castelao et al. 2005). Indeed, there are strong frontal activities along the MBGZ (Fig. 2a), which is parallel to the coastal boundary, and its surroundings are characterized by weak fronts. A similar coastal front separation phenomenon was also observed at Cape Blanco (Barth and Smith 1998). The influence of topography in frontogenesis is typically associated with other factors, such as SST and air-sea interaction (Chen et al. 2003). Water columns with different depths respond to surface cooling or warming differently such that a front may generate in regions with a sharp bathymetric gradient (Huang et al. 2005). The topography is changing rapidly in area 5 leading to difference in heat content between the shallow and deep water. Consistently, prominent shelf fronts are identified that distribute parallel to the bottom topography. This can also be revealed by the high correlation between the anomalous FP and SST in area 4 and 5 (Figs. 9 and 10).

Because of the overall high SST in the entire region, the front in area 4 is hardly observed during summer. In addition, the cold current from the north may lead to a higher SST gradient during winter, which results in a higher FP (Fig. 9d). Areas 3 and 5 are in the north of Changjiang river, and the SST in these areas varies considerably compared with those in the south (Fig. 5). Notably, the SST variation and FP are higher in area 5 compared to that in area 3. Because of the complicated water circulation in this area, the northern monsoon drives the coastal current to the south (Wei et al. 2011) where higher local SST leads to a higher FP (Fig. 10c).

Frontal areas are generally combined with strong turbulence induced by convection and diffusion. Nutrition or other materials in the subsurface may ascend to the upper layer, influencing the air-sea interaction and accelerating biochemical processes (Acha et al. 2004; Woodson and Litvin 2015). High concentrations of nutrients or essential materials for aquatic organisms can attract fish; Hu et al. (2012) proved that more fish are caught near coastal fronts. Huang et al. (2010) analyzed the spawning and overwintering grounds of anchovy in the Yellow and East China seas and concluded that the grounds of major commercial fisheries correlate well with fronts. Thus, a region with high frontal activity is associated with increased primary production. In addition, violent turbulence may also result in ascension of pollutants, such as plastics or microplastics, to the surface of the sea (Thompson 2004). Tanabe et al. (1991) illustrated that oceanic pollutants accumulate in frontal areas. However, with a change in the driving factor such as the flow of Changjiang River, wind, and SST (Liu and Feng 2012; Xuan et al. 2012), front distribution may vary. It is necessary to focus on the frontal zone and its driving factor to understand the oceanic pollutant distribution and concentration.

In summary, the coastal fronts in the ECS are greatly impacted by the alongshore wind, river discharge, air-sea heat fluxes, current, SST, and topography, though these factors contribute differently in different regions. North of the Changjiang River, the shelf fronts are mainly generated via SST-induced air-sea heat fluxes, which is largely determined by the topography. The coastal fronts are influenced by a combination of the alongshore wind and SST, due to the confluence of currents of different temperature and upwelling caused by the alongshore wind. Similarly, the front in the Hangzhou Bay is also correlated with the alongshore wind, which induces upwelling and outcrops cold subsurface water. South of the Changjiang River, the driving force for the shelf front is the alongshore wind and current. The abrupt change in topography regulates the flow of the Taiwan warm current, which induces fronts in offshore regions. The wind accelerates the ECS coastal current from north to south and subsequently enhances the front. For the coastal front, the river discharge influence is more obvious, which may due to the difference of river water temperature and ambient SST. However, validation, such as field observation, is still required to fully understand the regional dynamics in future. The frontal zone is typically associated with high primary and secondary production, which can influence fisheries. Convergence within a frontal zone may concentrate oceanic pollutants, e.g., microplastics. The better understanding of frontogenesis and front distribution presented in this study is helpful in the analysis of fisheries development and coastal pollution control.

Acknowledgments We greatly appreciate the Changjiang Water Resources Committee for sharing the river discharge data, the National Aeronautics and Space Administration (NASA) for sharing the satellite dataset (https://podaac-tools.jpl.nasa.gov/), and the European Center for Medium-Range Weather Forecasts (ECMWF) for releasing the ERA-Interim reanalysis product.

This study is supported by the Fundamental Research Funds for the provincial university (no. 2019J00019), the Scientific Research Fund of the Second Institute of Oceanography, Ministry of Natural Resources, China (no. HYGG2002), the National Natural Science Foundation of China (nos. 41806026 and 51909237), and the Project of State Key Laboratory of Satellite Ocean Environment Dynamics, Second Institute of Oceanography, MNR (no. SOEDZZ2102).

References

Acha EM, Mianzan HW, Guerrero RA, Favero M, Bava J (2004) Marine fronts at the continental shelves of austral South America: physical and ecological processes. J Mar Syst 44:83–105

Barth JA (1989) Stability of a coastal upwelling front: 1. model development and a stability theorem. J Geophys Res Oceans 94(C8):10844–10856

Barth JA, Smith RL (1998) Separation of a coastal upwelling jet at Cape Blanco, Oregon, USA. S Afr J Mar Sci 19(1):5–14

Beardsley RCR, Limeburner HY, Cannon GA (1985) Discharge of the Changjiang (Yangtze River) into the East China Sea. Continental Shelf Research 4:57–76

Belkin I, Cornillon P (2003) SST fronts of the Pacific coastal and marginal seas. Pacific Oceanogr 1:90–113

Belkin IM, Cornillon PC, Sherman K (2009) Fronts in large marine ecosystems. Prog Oceanogr 81:223–236

Briscoe MG, Johannessen O, Vincenzi S (1974) The maltese oceanic front: a surface description by ship and aircraft. Deep-Sea Res Oceanogr Abstr 21(4):247–262

Browne MA, Galloway T, Thompson R (2007) Microplastic - an emerging contaminant of potential concern? Integr Environ Assess Manag 3(4):559–561

Cao L, Kania PW, Buchmann K (2018) Particle effects on fish gills: an immunogenetic approach for rainbow trout and zebrafish. Aquaculture 484:98–104

Castelao RM, Barth JA (2005) Coastal ocean response to summer upwelling favorable winds in a region of alongshore bottom topography variations off Oregon. J Geophys Res 110:C10S04

Castelao RM, Wang Y (2014) Wind-driven variability in sea surface temperature front distribution in the California Current System. J Geophys Res 119:1861–1875

Castelao RM, Barth JA, Mavor TP (2005) Flow-topography interactions in the northern California Current System observed from geostationary satellite data. Geophys Res Lett 32:L24612

Cayula JF, Cornillon P (1995) Multi-image edge detection for SST images. J Atmos Ocean Technol 12(4):821–829

Chelton DB, Freilich MH (2005) Scatterometer-based assessment of 10-m wind analyses from the operational ECMWF and NCEP numerical weather prediction models. Mon Weather Rev 133(2):409–429

Chen CA (2008) Distributions of nutrients in the East China Sea and the South China Sea connection. J Oceanogr 64(5):737–751

Chen TW, Zhao CN (1985) Runoff, sediment transport and its influence on the coast of major rivers in China. Acta Oceanol Sin 7(4):460–471

Chen D, Liu WT, Tang WQ, Wang ZR (2003) Air-sea interaction at an oceanic front: implications for frontogenesis and primary production. Geophys Res Lett 30(14):1745

Chen X, Li G, Feng B, Tian S (2009) Habitat suitability index of chub mackerel (Scomber japonicus) from July to September in the East China Sea. J Oceanogr 65(1):93–102

Chen HH, Qi Y, Wang Y, Chai F (2019) Seasonal variability of SST fronts and winds on the southeastern continental shelf of Brazil. Ocean Dyn 69(11):1387–1399

Esaias WE, Abbott MR, Barton I (1998) An overview of MODIS capabilities for ocean science observations. EEE Trans Geosci Remote Sens 36:1250–1265

Fang G, Zhao B, Zhu Y (1991) Water volume transport through the Taiwan strait and the continental shelf of the East China Sea measured with current meters. Elsevier Oceanogr Series 54:345–358

Guan B, Chen S (1964) Current system in the marginal seas of China. In: National Oceanographic Comprehensive Survey Report, vol 5, pp 1–85

Hannachi A, Jolliffe IT, Stephenson DB (2007) Empirical orthogonal functions and related tecchniques in atmospheric science: a review. Int J Climatol 27:1119–1152

He SY, Huang DJ, Zeng DY (2016) Double SST fronts observed from MODIS data in the East China Sea off the Zhejiang–Fujian coast, China. J Mar Syst 154:93–102

Hickox R, Belkin I, Cornillon P, Shan Z (2000) Climatology and seasonal variability of ocean fronts in the East China, Yellow and Bohai Seas from satellite SST data. Geophys Res Lett 27:2945–2948

Hu CW, Lan KW, Hiroshi K, Lee MA, Lu HJ, Teruhisa S, Kohtaro H, Futoki S (2012) Relationship between albacore (Thunnus alalunga) fishing grounds in the Indian Ocean and the thermal environment revealed by cloud-free microwave sea surface temperature. Fish Res 112(1):1–7

Huang D, Fan X, Xu D, Tong Y, Su J (2005) Westward shift of the Yellow Sea warm salty tongue. Geophys Res Lett 32(24):348–362

Huang D, Zhang T, Zhou F (2010) Sea-surface temperature fronts in the Yellow and East China Seas from TRMM microwave imager data. Deep-Sea Res II Top Stud Oceanogr 57:1017–1024

Huang RH, Liu Y, Feng T (2013) Characteristics and causes of the interecadal jump of summertime moonsoon rainfall and circulation in eastern China occurred in the late 1990s. Chin Sci Bull 58(8):617–628

Huh OK (1982) Satellite observations and the annual cycle of surface circulation in the Yellow Sea, East China Sea, and Korea Strait. La Mer 20:210–222

Hwang JH, Van SP, Choi BJ, Chang YS, Kim YH (2014) The physical processes in the Yellow Sea. Ocean Coast Manag 102:449–457

Kaihatu JM, Handler RA, Marmorino GO, Shay LK (1998) Empirical orthogonal function analysis of ocean surface currents using complex and real-vector methods. J Atmos Ocean Technol 15:927–941

Kok JM, Valk C, Kester THM, Goede E, Uittenbogaard RE (2001) Salinity and temperature stratification in the rhine plume. Estuar Coast Shelf Sci 53(4):467–475

Legeckis R (1978) A survey of worldwide sea surface temperature fronts detected by environmental satellites. J Geophys Res 83:4501–4522

Lian E, Yang SY, Wu H, Yang CF, Li C, Liu JT (2016) Kuroshio subsurface water feeds the wintertime Taiwan Warm Current on the inner East China Sea shelf. J Geophys Res Oceans 121:4790–4803

Liu BC, Feng L (2012) An observational analysis of the relationship between wind and the expansion of the Changjiang river diluted water during summer. Atmos Ocean Sci Lett 5(5):384–388

Liu Z, Hou Y (2012) Kuroshio front in the East China Sea from satellite sst and remote sensing data. Geosci Remote Sens Lett IEEE 9(3):517–520

Ma J, Qiang FL, Xia CS, Yang YZ (2004) Tidal effects on temperature front in the Yellow Sea. Chin J Oceanol Limnol 22(3):314–321

Marmorino GO, Shen CY, Allan N, Askari F, Trizna DB, Trump CL, Shay LK (1998) An occluded coastal oceanic front. J Geophys Res 103(C10):21587–21600

O'Neill L, Chelton D, Esbensen S (2010) The effects of SST-induced surface wind speed and direction gradients on midlatitude surface vorticity and divergence. J Clim 23(2):255–281

Palma ED, Matano RP (2009) Disentangling the upwelling mechanisms of the south Brazil Bight. Continental Shelf Research 29:1525–1534

Pan YQ, Liang XS, Huang SS (1997) The evolution of the East China Sea dense water circulation and its influence on the mixing water diffusing off Changjiang mouth. Dohai Marine Sci 15:15–24 (In Chinese)

Qiao F, Yang Y, Lu X, Xia C, Chen X, Wang B, Yuan Y (2006) Coastal upwelling in the East China Sea in winter. J Geophys Res 111:1–11

Rao S, Pringle J, Austin J (2011) Upwelling relaxation and estuarine plumes. J Geophys Res Oceans 116:C09023

Renan PR, Bezerra MOM, Vinzón SB (2009) Dynamics of the saline front in the northern channel of the amazon river - influence of fluvial flow and tidal range (Brazil). J Coast Res 2(56):1414–1418

Shi R, Chen J, Guo X, Zeng L, Li J, Xie O, Wang X, Wang DX (2017) Ship observations and numerical simulation of the marine atmospheric boundary layer over the spring oceanic front in the northwestern South China Sea. J Geophys Res Atmos 122(7):3733–3753

Smith S, Roman M, Prusova I, Wishner K, Gowing M, Codispoti LA, Flagg C (1998) Seasonal response of zooplankton to monsoonal reversals in the Arabian Sea. Deep-Sea Res II Top Stud Oceanogr 45(10–11):2369–2403

Su J (2001) A review of circulation dynamics of the coastal oceans near China. Acta Oceanol Sin 23:1–16

Su JL, Wang K (1989) Changjiang river plume and suspended sediment transport in Hangzhou Bay. Cont Shelf Res 9(1):93–111

Tanabe S, Nishimura A, Hanaoka S, Yanagi T, Takeoka H, Tatsukawa R (1991) Persistent organochlorines in coastal fronts. Mar Pollut Bull 22(7):344–351

Teague WJ, Jacobs GA (2000) Current observations on the development of the Yellow Sea Warm Current. J Geophys Res 105:3401–3411

Thompson RC (2004) Lost at sea: where is all the plastic? Science 304(5672):838–838

Tseng C, Lin C, Chen S, Shyu C (2000) Temporal and spatial variations of sea surface temperature in the East China Sea. Cont Shelf Res 20(4):373–387

Ullman DS, David PC, Peter C (1999) Satellite-derived sea surface temperature fronts on the continental shelf off the northeast U.S. coast. J Geophys Res 104(C10):23459–23478

Waddell E, Karpen J, Debrule P (1979) Field study of pollutant migration in the vicinity of a coastal front. Oceans IEEE:635–641

Wang Y, Castelao R (2016) Variability in the coupling between sea surface temperature and wind stress in the global coastal ocean. Cont Shelf Res 125:88–96

Wang B, Wang X (2007) Chemical hydrography of coastal upwelling in the East China Sea. Chin J Oceanol Limnol 25:16–26

Wang Y, Castelao RM, Yuan Y (2015) Seasonal variability of alongshore winds and sea surface temperature fronts in Eastern Boundary Current. J Geophys Res 120:2385–2400

Wang Y, Yu Y, Zhang Y, Zhang H-R, Chai F (2020) Distribution and variability of sea surface temperature fronts in the South China Sea. Estuar Coast Shelf Sci 240:106793

Wei QS, Yu ZG, Ran XB, Zang JY (2011) Characteristics of the western coastal current of the Yellow Sea and its impact on material transportation. Adv Earth Sci 26(2):145–155

Williams JW, Weingartner TJ, Albert JH (2010) Idealized two-dimensional modeling of a coastal buoyancy front, or river plume, under downwelling-favorable wind forcing with application to the Alaska coastal current. J Phys Oceanogr 40:279–294

Woodson CB, Litvin SY (2015) Ocean fronts drive marine fishery production and biogeochemical cycling. Proc Natl Acad Sci 112:1710–1715

Wu H, Deng B, Yuan R, Hu J, Gu J, Shen F (2013) Detiding measurement on transport of the Changjiang-derived buoyant coastal current. J Phys Oceanogr 43:2388–2399

Wu C, Wang YL, Lin YF, Chao SY (2017) Intrusion of the Kuroshio into the South and East China Seas. Sci Rep 7(1):7895–7895

Xuan JL, Huang DJ, Zhou F, Zhu XH, Fan X (2012) The role of wind on the detachment of low salinity water in the Changjiang estuary in summer. J Geophys Res Oceans 117:C10004

Yang D, Huang RX, Yin B, Feng X, Chen H, Qi J, Xu L, Shi Y, Cui X, Gao G, Benthuysen JA (2018) Topographic beta spiral and onshore intrusion of the Kuroshio Current. Geophys Res Lett 45(1):287–296

Yu Y, Wang Y, Cao L, Chai F (2020) The ocean-atmosphere interaction over a summer upwelling system in the South China Sea. J Mar Syst 208:103360

Yuan YC, Su JL, Xia S (1987) Three-dimensional diagnostic calculation of circulation over the East China Sea shelf. Acta Oceanol Sin 6:36–50

Zaneveld JRV, Pak HJ (1979) Optical and particulate properties at oceanic fronts. J Geophys Res 84(C12):7781–7790

Zhang X, Lin CM, Gao S, Dalrymple RW, Qu CW, Yin Y, Li YL (2013) Sedimentary sequence and distribution pattern of filling in Qiantang river incised valley. J Palaeogeogr 15(6):839–852

Zheng QA, Klemas V (1982) Determination of winter temperature patterns, fronts, and surface currents in the Yellow Sea and East China Sea from satellite imagery. Remote Sens Environ 12:201–218

Zhu J, Chen C, Li C, Lin H (2004) Does the Taiwan warm current exist in winter? Geophysical Research Letters 31:L12302

Zhu Y, Sun J, Wang Y, Li S, Xu T, Wei Z, Qu T (2019) Overview of the multi-layer circulation in the South China Sea. Prog Oceanogr 175:171–182